1
2
3

Species Tailoured Contribution of Volumetric Growth and Tissue Convergence to Posterior Body Elongation in Vertebrates

4

5   **Running title:** Growth and Posterior Elongation

6   **Keywords:** Multi-scalar morphometric analysis, Zebrafish, Mouse, Lamprey,

7   Dogfish, energy supply.

8

9   Ben Steventon[1,2*], Fernando Duarte[1,3], Ronan Lagadec[4,6], Sylvie Mazan[4,6], Jean-

10   François Nicolas[1], and Estelle Hirsinger[1,5]

11   [1]Department of Developmental and Stem Cell Biology, Institut Pasteur, 25 rue du Doctor Roux, Paris,

12   France.

13   [2]Present address: Department of Genetics, University of Cambridge, Cambridge CB2 3EH, UK

14   [3]Present address: Centre de Biologie du Developpement, UMR 547 CNRS. Universite Paul Sabatier,

15   118 Route de Narbonne, 31400 Toulouse, France.

16   [4]Development and Evolution of Vertebrates, CNRS-UPMC-UMR 7150, Station Biologique, Roscoff,

17   France

18   [5]Present address: IBPS - Laboratoire de Biologie du Développement (LBD), CNRS, UPMC, UMR

19   7622, INSERM ERL U1156, 9 Quai Saint-Bernard, 75252 Paris Cedex 05 France

20   [6]CNRS, Sorbonne Universités, UPMC Univ Paris 06, UMR7232, Observatoire Océanologique,
21   Banyuls, France.
22

23   *Corresponding author

24

1 **Abstract.**

2 **Posterior body elongation is a widespread mechanism propelling the**

3 **generation of the metazoan body plan. The posterior growth model predicts**

4 **that a posterior growth zone generates sufficient tissue volume to elongate the**

5 **posterior body. However, there are energy supply-related differences between**

6 **vertebrates in the degree to which growth occurs concomitantly with**

7 **embryogenesis. By applying a multi-scalar morphometric analysis in zebrafish**

8 **embryos, we show that posterior body elongation is generated by an influx of**

9 **cells from lateral regions, by convergence-extension of cells as they exit the**

10 **tailbud, and finally by a late volumetric growth in the spinal cord and**

11 **notochord. Importantly, the unsegmented region does not generate additional**

12 **tissue volume. FGF inhibition blocks tissue convergence rather than**

13 **volumetric growth, showing that a conserved molecular mechanism can**

14 **control convergent morphogenesis through different cell behaviours. Finally,**

15 **via a comparative morphometric analysis in lamprey, dogfish, zebrafish and**

16 **mouse, we propose that elongation via posterior volumetric growth is linked to**

17 **increased energy supply and is associated with an overall increase in**

18 **volumetric growth and elongation.**

19

20 **Introduction**

21 Axial elongation is a widespread mechanism propelling the generation of the

22 metazoan body plan. Despite the importance of this essential event in the formation

23 of the body axis, we know little about the individual cell behaviours driving

24 elongation. This is not surprising given the number of cell behaviours that can lead to

1   the elongation of such a complex, multi-tissue structure. Elongation mechanisms can

2   be separated into two categories. Firstly, those that result in a volumetric increase of

3   the tissue such as cell growth, deposition of extracellular matrix or the decrease in

4   local density by an increase in cell motility, as has been shown in chick (Bénazéraf et

5   al., 2010). Cell proliferation alone (in the absence of cell growth) will not generate

6   volumetric growth. Secondly, those cell behaviours that lead to tissue convergence

7   (i.e. a directional deformation of a tissue in the absence of volumetric growth) such

8   as cell rearrangement, orientated cell division or cell shape change. Vertebrate

9   embryos develop in vastly different nutritive environments that have a large impact

10   on the relative degree of growth occurring during development (O'Farrell, 2015). This

11   is likely to have an impact on the degree to which volumetric growth contributes to

12   elongation. This is especially the case for externally developing embryos with limited

13   energy supply, such as the zebrafish, that must develop a full axis in order to swim

14   and find food prior to overt growth.

15

16   A widely accepted model for vertebrate posterior body elongation is that of posterior

17   growth, where new cells are continually added from the posterior tip of the elongating

18   posterior body. A posterior proliferative zone is thought to drive this process by

19   providing new cells to populate the posterior tissues, the mesoderm and spinal cord

20   in particular (Beddington, 1994; Bouldin et al., 2014; Cambray and Wilson, 2002;

21   Mathis and Nicolas, 2000; McGrew et al., 2008; Nicolas et al., 1996; Selleck and

22   Stern, 1991; Martin and Kimelman, 2009; Martin and Kimelman, 2012; Neijts et al.,

23   2013). However, in the absence of growth behaviours, it is not clear whether this

24   posterior proliferative zone can generate sufficient volume increase at the whole

1 structure level to contribute to the elongation of the posterior body. The zebrafish

2 *emi1* mutant, in which cell divisions are blocked from the beginning of gastrulation

3 (Riley et al., 2010; Zhang et al., 2008), is shortened by around 30% but exhibits a

4 non-truncated axis with its full complement of somites. In the scenario where a

5 posterior proliferative zone would be the major actor, one would expect a truncation

6 of the axis. Several non-growth cell behaviours have been proposed to drive

7 elongation via tissue convergence, particularly in anamniote embryos such as

8 zebrafish. Gastrulation-like cell rearrangements such as convergence-extension,

9 together with novel cellular movements have been observed during zebrafish

10 posterior body elongation (Kanki and Ho, 1997). Blocking FGF signalling leads to an

11 inhibition of cellular flow from the tailbud and the disruption of axis elongation

12 (Lawton et al., 2013).

13

14 To generate elongation of the posterior body, the posterior growth model predicts

15 that additional tissue volume is generated from the unsegmented region. To address

16 this in zebrafish and to compare to other vertebrates, we aim to determine the

17 relative contribution of volumetric growth (i.e. increase in tissue volume) vs. tissue

18 deformation (i.e. elongation in the absence of volume increase) to posterior body

19 elongation. We show that posterior body elongation in zebrafish is generated by an

20 influx of cells from lateral regions, by convergence-extension of cells as they exit the

21 tailbud, and finally by a late volumetric growth in the spinal cord and notochord. The

22 unsegmented region does not generate additional tissue volume. FGF signalling

23 controls convergence within the tailbud and PSM. Our comparative study shows that

24 posterior volumetric growth is associated with an internal mode of development.

1

Results

The prospective posterior body is not restricted to the tailbud.

Posterior body elongation starts with the primitive streak or blastopore closure and ends with the end of somitogenesis. In zebrafish, the anterior body that corresponds to the anterior trunk is already established by the late gastrula as the anterior trunk somites (1-12) are already present within the pre-somitic mesoderm (Kanki and Ho, 1997). Subsequently, the remaining 20 segments of the body form in an anterior to posterior fashion through the process of posterior body elongation, the posterior trunk spanning somites 13-17 and the tail somites 18-32. Previous studies have focused on cells within the tailbud (Kanki and Ho, 1997; Lawton et al., 2013). However the limits of the posterior body territory are unknown from the end of gastrulation up to the 12-somite stage, when the tailbud has lifted from the yolk and formed a definable prominence. We mapped the limits of the prospective posterior body between the end of gastrulation and 12-somite stage by generating 12 independent movies in which clusters of 10-20 cells were photolabeled at 90% epiboly and tracked until their incorporation into the embryo axis using Imaris. Photolabelling was achieved with the use of a nuclear localised KikGR protein (S1 Movie), that switches from green to red fluorescence upon UV exposure (Hatta et al., 2006). We find that cells lateral to the tailbud converge and enter the tailbud (blue; Fig. 1A-C). Cells lateral to the elongating axis enter directly into both the spinal cord (yellow; Fig1A-C) and pre-somitic mesoderm (PSM; red; Fig. 1A-C) without having passed through the tailbud (S1 Movie).

1   To determine the extent to which non-tailbud cells contribute to the embryonic axis,

2   we tracked photolabelled cells in movies visualised from the lateral view (S2 Movie;

3   Fig. 1D-F). Surprisingly, we find that cells contribute to the somitic mesoderm up until

4   the 17th somite, without having first passed through the tailbud region (red tracks in

5   S2 Movie; Fig. 1D-F). Cells labelled just caudal to prospective 17th somite enter into

6   the tailbud prior to the PSM (dark blue tracks in S2 Movie; Fig. 1D-F). As somite 17

7   marks the trunk-tail transition, these results suggest that lateral cells populate the

8   posterior trunk by undergoing convergence and extension without transiting through

9   the tailbud, and that tailbud cells generate the tail only.

10

11 To determine whether elongation at these early stages involves cell proliferation, we

12 calculated the proliferation rate within each photolabelled cell clone between the

13 90% epiboly and 12-somite stages (Fig. 1G). The proliferation rate being around 0.1

14 cell/hour on average, only an average of 0-2 additional cells are generated within

15 clones fated towards epidermis, tailbud, spinal cord and the somitic mesoderm,

16 demonstrating that cell proliferation is not a major driving force in early elongation.

17 As a proxy for cell intercalation, we calculated an index of clone dispersion,

18 measured as the mean increase in inter-nuclear distance of neighbouring cells

19 between the 90% epiboly and 12-somite stages (Fig. 1H). The index of dispersion is

20 high for all axial clones, particularly for cell clones fated towards the spinal cord

21 (mean increase in internuclear distance: 50µm), tailbud (18µm) and PSM (11 µm),

22 with little cell dispersion occurring for the epidermis (5.5 µm). This demonstrates that

23 a considerable degree of cell intercalation is occurring within lateral cells to reach the

24 axial tissues.

1

2 Together, these results demonstrate that the prospective posterior body region at

3 late gastrula stage is much larger than previously thought and not restricted to the

4 tailbud, which prompted us to examine the contributions of volumetric growth and

5 tissue deformation at the level of the whole posterior body.
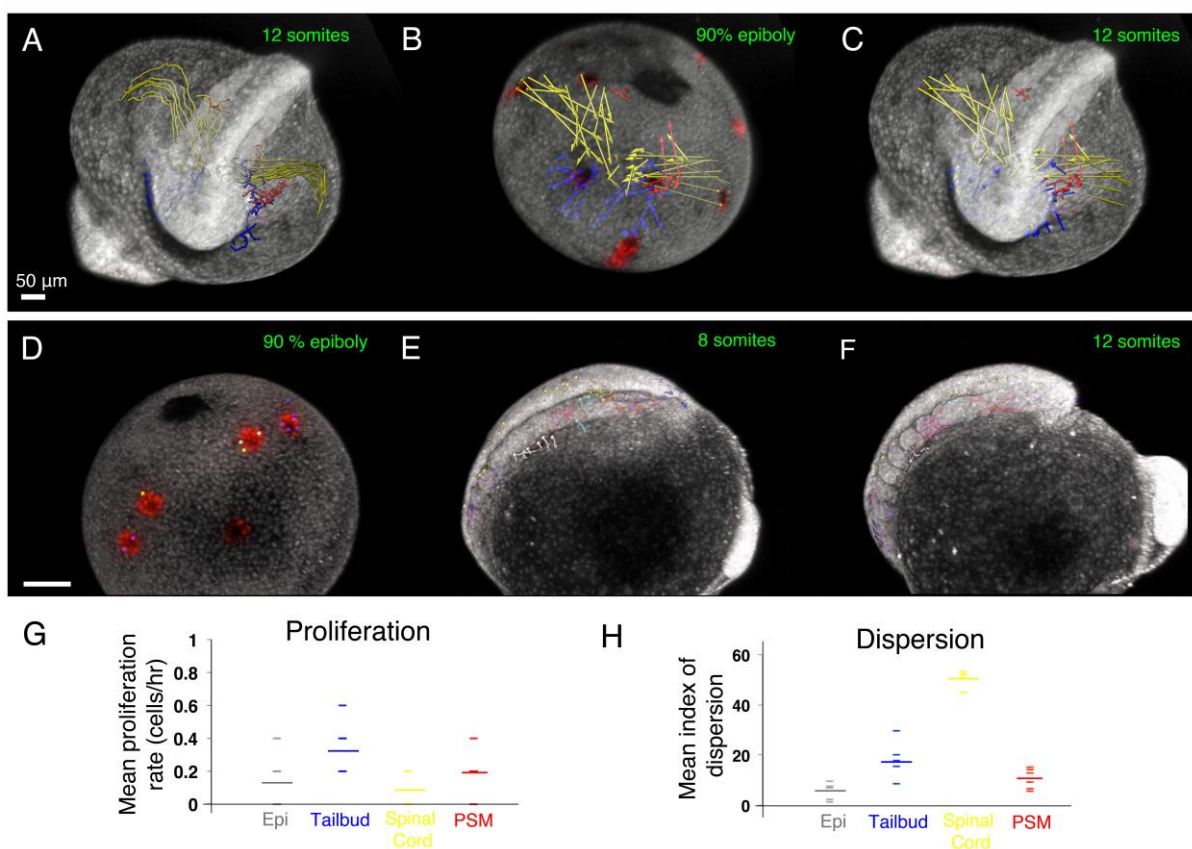
6

7 **Figure 1. Convergence of lateral cells contributes to the elongating posterior body.**

8   (A-C) Tracks (A) and displacement vectors (B,C) of spinal cord (yellow), tailbud (blue) and PSM (red)

9 precursors from automated tracking of photolabeled nuclei from the 90% epiboly to the 12-somite

10 stage. (D-F) Tracks of cells from the 90% epiboly to the 12-somite stage. (G) Proliferation rate,

11 expressed as the number of additional cells generated divided by the time interval (5 hrs), within

12 clones fated towards the Epidermis (mean 0.13 cells/hr, n=53), Tailbud (mean 0.36 cells/hr, n=53),

13 Spinal Cord (mean 0.04 cells/hr, n= 85) and PSM (mean 0.2 cells/hr, n=74). (H) Index of dispersion

14 (mean increase in inter-nuclear distance between neighbouring cells) for cells fated towards the

Epidermis (mean 5.56μm, n=53), Tailbud (mean 18μm, n=53), Spinal Cord (mean 50μm, n= 85) and PSM (mean 11μm, n=74). Small dashed lines show values from 5 independent movies. Large dashed lines mark the mean.

Elongation occurs through extensive convergence with a late phase of volumetric growth.

To determine the relative contributions of volumetric growth and tissue deformation to elongation throughout the entire process, we built 3D surface reconstructions of the posterior body and its presumptive territory from the 3- to the 32-somite stages using our early fate map and fixed samples at later stages (Fig. 2A; S3 Movie). From these, we extracted quantitative information on volume, length, width and height changes. We did not observe an increase in volume until the 24-somite stage (Fig. 2B; grey). However, there is continual elongation despite the absence of volumetric growth (Fig. 2C; grey). Up until the 24-somite stage (purple to yellow lines in Fig. 2D, E), there is a four-fold decrease in width (Fig. 2D) along with an increase in height (Fig. 2E), suggesting that convergence in width is contributing both to an increase in length and height. These results demonstrate that whilst volumetric growth may contribute to elongation between the 24 and 32-somite stages (growth phase), much of the earlier stages (non-growth phase) of elongation are driven by convergence and extension.
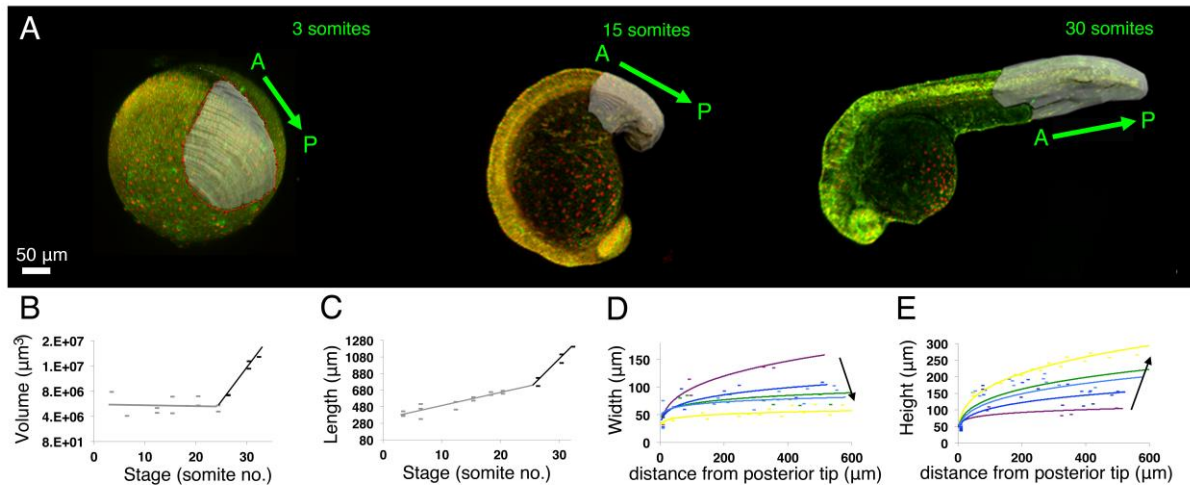
Fig. 2. Posterior body elongation in zebrafish occurs firstly in the absence of volumetric growth followed by a later volumetric growth phase.

(A) Surface reconstructions (grey region) of the posterior body through posterior body elongation. Embryos previously injected with nuclear mCherry and membrane eGFP mRNAs in lateral view with A and P marking anterior and posterior poles. (B-C) Plots of volume (B; n=21) and length (C; n=21) against time (number of somites). Grey points/trendlines: 3- and 24-somite stages. Black points/trendlines: 24-32 somite stages. (D-E) Width (D) and height (E) against distance from posterior tip of the tail to where each measurement was taken. Curves each correspond to a developmental stage (number of somites). Colour code: purple= 12 somites (s) (n=5), dark blue= 15s (n=8), light blue= 18s (n=7), green= 20s (n=12), yellow= 24s (n=17). Data points show individual measurements, n=total number of measurements from 3 embryos per stage.

No additional tissue volume is generated from the unsegmented region in zebrafish.

We next wanted to determine in which portion of the posterior body volumetric growth is generated: either in the unsegmented region that includes the tailbud, or within the segmented region. We took embryos previously injected with mRNA encoding cytoplasmic KikGR, photolabelled one or the other region and performed 5 h-long time-lapse imaging (Fig. 3A,D,G, S4 Movie). As cells are exiting the tailbud

9

1   and entering the PSM, we saw considerable mixing of labelled cells with unlabelled

2   cells of the rostral PSM. For our length measurements, we thus took the most

3   anterior and the most posterior photolabeled (i.e red) cells. For volume

4   measurements, we segmented the photoconverted (i.e. red) signal only. Although

5   the unsegmented region contributes to elongation (2.67 fold increase; Fig. 3B), this

6   region does not increase in volume during both no-growth and growth phases (0.98

7   fold change; Fig. 3C). We then photolabelled the unsegmented region at the 21-

8   somite stage and measured its volume through to the completion of elongation (Fig.

9   3D). This further confirmed the absence of unsegmented region volumetric growth

10   during the growth phase (Fig. 3F). However, this region continues to contribute to

11   elongation at these late stages, although to a lesser extent (1.61 fold increase; Fig.

12   3E). Unlike the unsegmented region, the segmented region (Fig. 3G) does undergo

13   both elongation (2.19 fold increase; Fig. 3H) and volumetric growth (1.25 fold

14   increase; Fig. 3I). Therefore, volumetric growth only occurs in the already segmented

15   region where differentiation is known to take place.
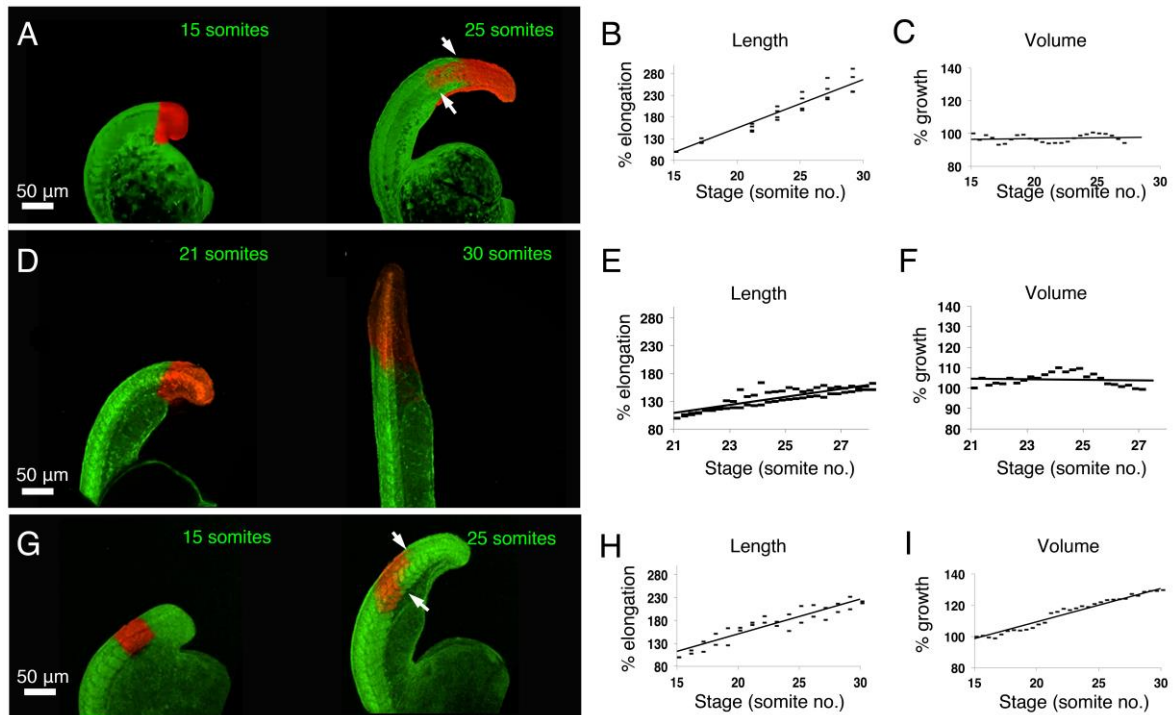
Figure 3. Volumetric growth only occurs within already segmented regions of the zebrafish posterior body.

(A, D, G) Stills from time-lapse movies of embryos injected at the one cell stage with KikGR mRNA and photo-labelled within the unsegmented region at the 15-somite (A) or 21-somite stage (D) or within the segmented region at the 15-somite stage (G). Embryos in lateral view with posterior to the top. (B, E, H) Photoactivated region length (% of initial length) plotted against time (number of somites), n(B)=25, n(E)=51, n(I)=29. (C, F, I). Photoactivated region volume (% of initial volume) plotted against time (number of somites), n(C)=25, n(F)=25, n(I)=31. White arrows in (A) indicate the displacement of labels within the somitic mesoderm (lower arrows) relative to the spinal cord (upper arrows). Data points show individual measurements, n=total number of measurements from 3 independent experiments.

Proliferation rapidly reaches a low level in the unsegmented region but continues into the growth phase in the segmented region.

11

1   We next sought to determine the amount of cell division that occurs within different

2   regions of the posterior body during elongation. To achieve this, we made use of the

3   zFUCCI green transgenic line that displays green fluorescent nuclei when in S/M/G2

4   phases of the cell cycle (Sugiyama et al., 2009). We injected these embryos at the

5   one cell stage with nuclear localised mCherry mRNA in order to mark all cell nuclei

6   (Fig. 4A). After segmentation of the region of interest, we calculated the percentage

7   of dividing cells as the number of green nuclei over the number of red nuclei in that

8   region. We first analysed the proliferation levels within the entire body (Fig. 4B; black

9   line) or within the tailbud (Fig. 4B; blue line) between the 15 and 22-somite stages.

10   While at early stages a comparable percentage of cell divisions occurred within the

11   tailbud as with the rest of the posterior body, this dropped off rapidly from the 14-

12   somite stage onwards, similar to what has been reported in Bouldin et al. (2014).

13

14   We next evaluated the percentage of dividing cells within the tailbud (Fig.4C; blue),

15   PSM (Fig.4C; red), somites (Fig.4C; orange), spinal cord (Fig.4C; yellow), notochord

16   (Fig.4C; purple) and blood precursors (Fig.4C; green) at the 20-, 25- and 30-somite

17   stages. Only few divisions were observed within the tailbud, and whilst some cells

18   (approx. 10%) of the PSM are dividing at the 20-somite stage, this rapidly drops as

19   somitogenesis proceeds. Proliferation levels are also low within the notochord, as

20   reported in Sugiyama et al. (2009). In contrast, the proliferation levels within the

21   spinal cord, somites and blood precursors are notably higher. Apart from the early

22   stages of elongation when they are similar, these results show that proliferation

23   levels are higher in the segmented region than in the unsegmented region.
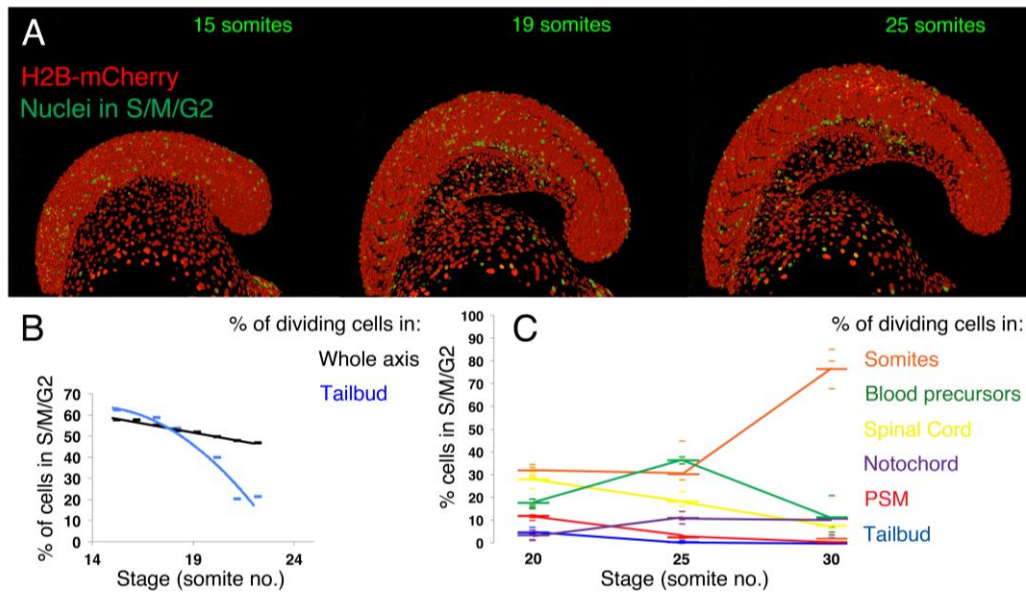
Figure 4. Proliferation rapidly reaches a low level in the unsegmented region. (A) Stills from a time-lapse of zFUCCI green embryos injected with nuclear mCherry mRNA. Plot of the percentage of nuclei in S/M/G2 (green) with respect to total nuclei (red) against time (number of somites), showing the posterior body as a whole (black line) and the tailbud (blue line). Trend was observed in 3 independent time-lapses. (C) Percentage of nuclei in S/M/G2 (green) with respect to total nuclei (red) in Tailbud (blue), PSM (red), Notochord (purple), Spinal cord (yellow), Blood precursors (green) and Somites (orange) at 20-, 25- and 30-somite stages. Small dashes show counts from 4 embryos fixed at each stage, large dashes display mean value.

Differential tissue contributions to both volumetric growth and convergence and extension.

To assess tissue specific differences in volumetric growth and convergence we photo-labelled small regions within the tailbud, PSM, somites and spinal cord (Fig. 5A-C) and quantified their percentage of volume increase and their length:width ratio over time (Fig. 5D,E). When compared to the whole posterior body measurements (Fig. 5D,E; black lines), the spinal cord contributes the most to volumetric growth

13

1 (Fig. 5B,D; blue). This tissue also has a large positive increase in the length:width

2 ratio (Fig 5B,E; S5 movie; blue), suggesting that either volumetric growth is

3 anisotropic (through oriented cell division or oriented growth of the cells) or that

4 additional cell rearrangements such as convergence-extension are leading to a

5 thinning of this structure. The cells in transit from the tailbud to the PSM contribute

6 the most to thinning and lengthening but in the absence of volumetric growth (Fig.

7 5C-E; S6 movie; green). Once cells have entered the PSM, little thinning and

8 lengthening occurs (Fig. 5B,E; S5 movie; yellow). This tissue also undergoes a slight

9 compaction during somite formation (Fig. 5B,D; yellow).

10

11 Inflation of the notochord by the formation of fluid-filled organelles has an important

12 role in the elongation of the zebrafish axis (Ellis et al., 2013). In line with this, we

13 observe a considerable increase in the volume of bounding-boxes surrounding

14 notochord photo-labels (Fig. 5D; purple; includes the organelle volume) without a

15 corresponding increase in the volume of the KikGR-labelled cytoplasm (Fig. 5D;

16 magenta; excludes the organelle volume). In addition to inflation and proliferation,

17 the notochord also undergoes convergence and extension (Glickman et al., 2003),

18 which is mirrored by an increase in length:width ratio (Fig. 5E; purple). However, as

19 cells begin to inflate, they do so in all directions, leading to a later decrease in

20 length:width ratio (Fig. 5E; purple).

21

22 The impact of these distinct tissues on the elongation of the posterior body as a

23 whole will depend on their initial size with respect to the whole posterior body. On

24 embryos previously injected with nuclear mCherry and membrane eGFP mRNAs, we

1   segmented the paraxial mesoderm, spinal cord and notochord at the 15-somite

2   stage and measured their volume as a proportion of the posterior body volume (S7

3   Figure). The paraxial mesoderm and spinal cord make up the largest portion of the

4   posterior body, at approx. 23% and 12% respectively, confirming their major

5   contribution to elongation. The notochord, at 1.9% of the whole posterior body

6   contributes to a much lesser extent than the former two tissues. The remaining

7   approx. 63% of the posterior body is divided up between inter-tissue components,

8   the non-neural ectoderm, the non-paraxial mesoderm and endodermal tissues which

9   all may be contributing to differing extents to elongation.

1
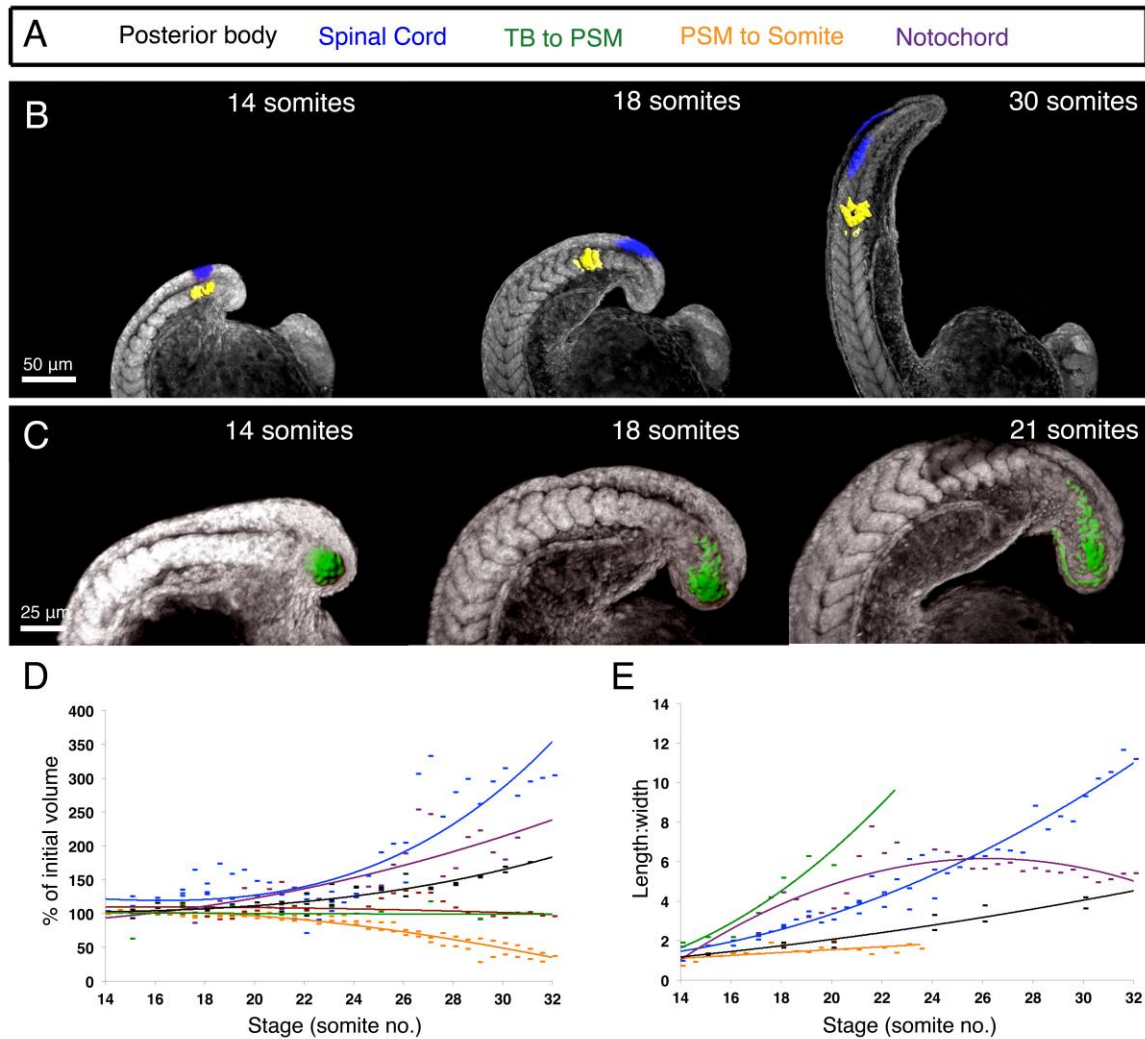
Figure 5. The spinal cord and notochord are the principal contributors to volumetric growth and the TB to PSM transiting cells to thinning and lengthening. (A) Different tissues are colour coded according to the key shown. (B, C) Stills from time-lapse movies of embryos injected at the one cell-stage with KikGR mRNA and photo-labelled in the spinal cord and in the PSM (B) or in the tailbud (TB) (C) at the 14-somite stage. (D, E) Plots of volume fold increase (D; n(Spinal cord)=51, n(notochord)=31, n(PSM to somites)=58, n(TB to PSM)=23) and length:width ratio (E; n(Spinal cord)=43, n(notochord)=30, n(PSM to somites)=17, n(TB to PSM)=12) of each photo-labelled region against time (number of somites). The red curve in D corresponds to volume fold increase of bounding-boxes surrounding notochord photo-labels. Data points show individual measurements, n=total number of measurements from embryos from three experiments.
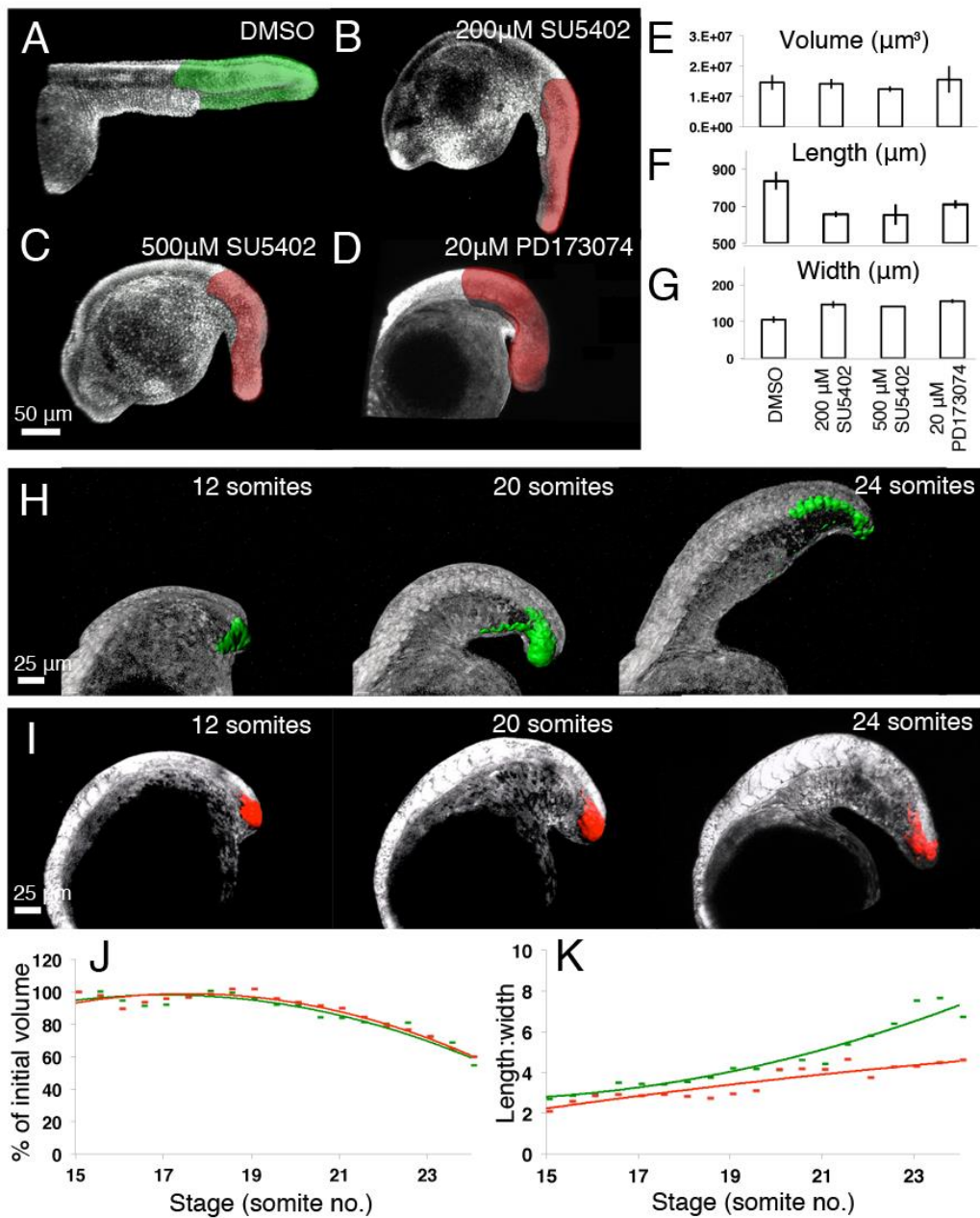
FGF signalling is required for convergence and extension, not posterior volumetric growth in zebrafish.

FGF signalling is known to be important for posterior body elongation across vertebrates (Bénazéraf et al., 2010; Bouldin et al., 2014; Diez del Corral and Storey, 2004; Olivera-Martinez et al., 2012; Lawton et al., 2013). We applied our morphometric approach to determine whether FGF signalling plays a role in volumetric growth and/or convergence during posterior body elongation in zebrafish. To circumvent effects on mesoderm induction and patterning as a consequence of inhibiting FGF signalling prior to the end of gastrulation, we added known inhibitors of FGF receptors (SU5402 and PD173074) at the 10-somite stage. Examination at the 32-somite stage lead to clear affects on posterior body morphology when compared to DMSO treated controls (Fig. 6A-D). Neither treatment affected posterior body volume (Fig. 6E, $p > 0.7$ in all cases). However, we did see a significant reduction in posterior body length (Fig. 6F, $p < 0.01$). This coincided with an increase in mean width (Fig. 6G, $p < 0.01$), suggesting that an inhibition of convergence and extension is the likely cause of posterior body shortening upon inhibition of FGF signalling. To test this, we repeated our photo-labellings of a small region of the tailbud at 12-somite stage in embryos cultured in DMSO (Fig. 6H) or together with PD173074 (Fig 6I), and monitored their volume increase and length:width ratio as they transit into the PSM. No effect was observed on the volume of the tailbud photo-labelled cells upon addition of PD173074 (Fig. 6J), however we did observe an inhibition of the length:width ratio increase that is normally observed for these cells (compare red to green lines in Fig. 6K).

1

2 To assess whether FGF inhibition is affecting cellular movements and/or cell

3 proliferation/apoptosis, we generated clones of photolabeled cells in the tailbud,

4 PSM or spinal cord at the 10-somite stage (Fig. 7A,C) and quantified their

5 length:width ratio (Fig. 7E) and cell number (Fig. 7F) at 26-somite stage (Fig. 7B,D)

6 in absence or presence of SU5402. While only a slight decrease was observed for

7 cells entering the somites (Fig. 7E; yellow) or within the spinal cord (Fig. 7E; blue), a

8 significant inhibition of the length:width ratio increase for cells that exit the tailbud

9 and enter the PSM was observed upon FGF receptor inhibition (Fig. 7E; green). No

10 effect on cell number was observed for FGF inhibition in any region examined (Fig.

11 7F). This last result was then confirmed by analysing cell divisions using the zFUCCI

12 line (Fig. 7G-I). SU5402 treatment did not lead to a significant change in the

13 percentage of dividing cells in the entire posterior body at either the 18- or 32-somite

14 stage (Fig. 7I). Nor did SU5402 treatment affect total cell number with the entire

15 posterior body at either the 18-somite stage (mean cell number = 1691 +/- 235 for

16 DMSO; 1693 +/- 253 for 200µM SU) or 32-somite stage (mean cell number = 2107

17 +/- 359 for DMSO; 2115 +/- 441 for 200µM SU). To ensure that our SU5402

18 treatment adequately blocks FGF signalling, even deep within the tailbud, we made

19 use of a high signal:noise ratio fluorescent *in situ* based approach (HCR) that allows

20 for the direct observation of mRNA transcripts by confocal microscopy (Choi et al.,

21 2010, 2014). Staining for *sprouty4* expression as a read-out for FGF signalling

22 activity reveals a strong expression in the tailbud (Fig. 7K). Upon addition of

23 SU5402, expression of *sprouty4* for is greatly reduced, confirming the efficacy of this

24 small molecule treatment (Fig. 7K). Taken together, these results demonstrate that

1   the role of FGF in zebrafish posterior body elongation is to control tissue

2   convergence as cells exit the tailbud and enter the PSM.

3

4   **Figure 6. FGF signalling is required for thinning and lengthening, not volumetric growth of the**

5   **zebrafish posterior body.** (A-D) Embryos injected at one-cell stage with nuclear mCherry mRNA and

6   incubated in either 500µM DMSO (A), 200µM SU5402 (B), 500µM SU5402 (C) or 20µM PD173074

7   (D) from the 10-somite stage until the 32-somite stage and imaged by confocal microscopy at 32-

somite stage. (E-G) Mean value of posterior body volume (E), length (F) and width (G) for each

condition at 32-somite stage. Error bars: +/- s.d. (H-I) Stills from time-lapse movies of embryos in

which small regions within the tailbud are photolabelled at 12-somite stage in the presence of 500µM

DMSO (H) or 20µM PD173074 (I). (J-K) Quantification of the volume (J) and length:width ratio (K) of

the photo-labelled region over time (number of somites). Green lines correspond the control situation

(500µM DMSO), red lines indicate treatment with PD173074.
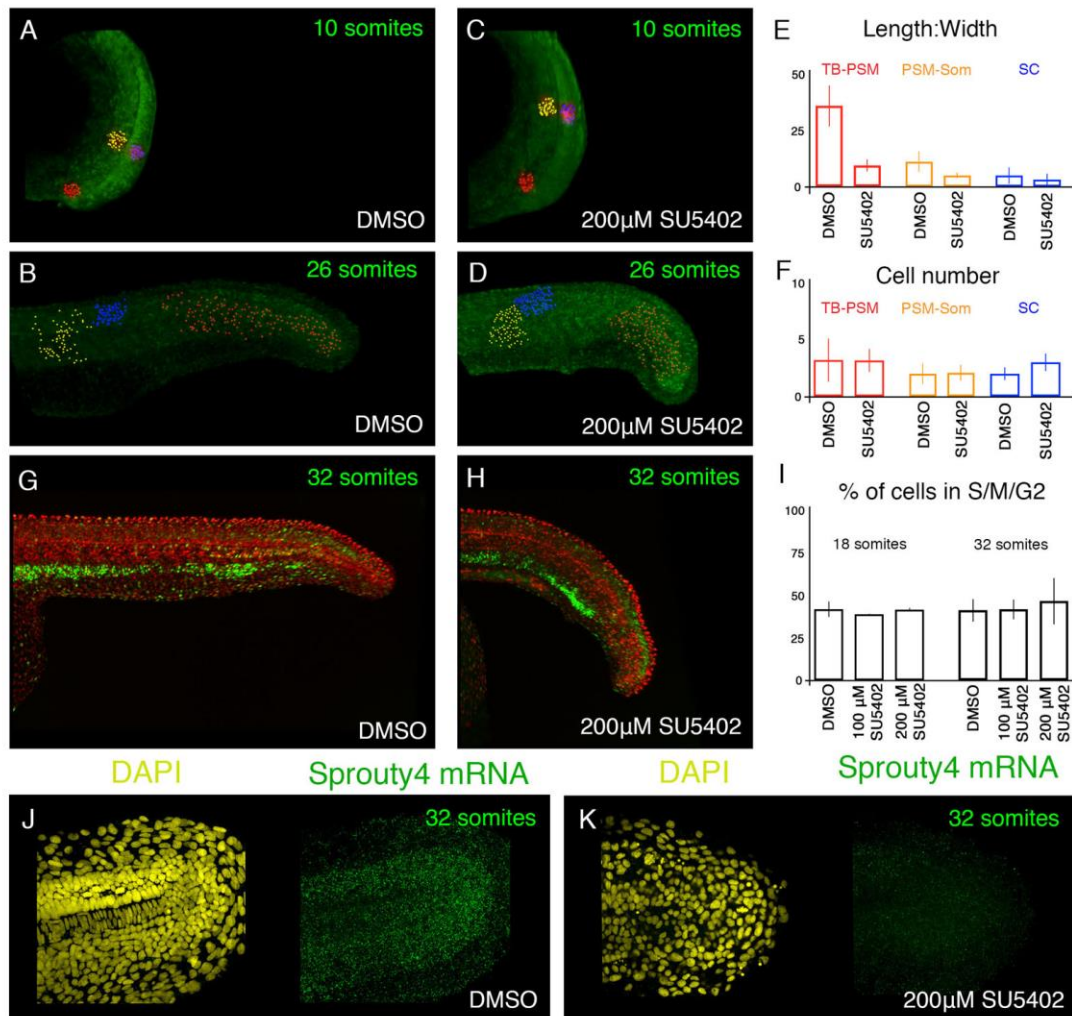
Figure 7. FGF signalling is required for cell movements and not cell proliferation. (A-D)

Embryos previously injected with nls-KikGR mRNA were incubated in either 500µM DMSO (A,B) or

200µM SU5402 (B,D). (E,F) Photolabels in tailbud (TB-PSM; red), PSM (PSM-Somites; yellow) or

spinal cord (SC; blue) were measured to display mean length:width ratio (E) and cell number (F).

Error bars: +/- s.d. (G,H). zFUCCI green embryos injected with nuclear mCherry mRNA and incubated

20

1   in either 500µM DMSO (G) or 200µM SU5402 (H) from the 10- to the 32-somite stage. (I) Mean

2   percentage of nuclei in S/M/G2 are plotted for each condition at 18- and 31-somite stages. Error bars:

3   +/- s.d. 3-5 embryos were analysed for each condition shown. (J,K) Fluorescent in situ hybridisations

4   for the immediate FGF response gene sprouty4 (green), together with counter-staining for nuclei with

5   DAPI (yellow) in the presence of 200µM SU5402 (K) or with DMSO only (J). Images are maximum

6   projections of a 10µm focal section through the embryonic midline to determine FGF inhibition deep

7   within the tissue of interest.

8

9

10 **Species tailoured contribution of volumetric growth to posterior body**

11 **elongation in vertebrates.**

12 The relatively small contribution of volumetric growth to the elongation of the

13 posterior body in zebrafish is striking and prompted us to determine whether the lack

14 of posterior volumetric growth was characteristic of the external development of

15 anamniote embryos. Therefore we compared our morphometric measurements in

16 zebrafish (Fig. 8C,E) to the amniote mouse embryo (Fig. 8D,E) and to a basal

17 anamniote vertebrate, the lamprey (Fig. 8A,E). As a further comparison, we analysed

18 the anamniote dogfish that is evolutionarily basal to teleost fish (Fig. 8B,E) but

19 develops within an egg case and with a large yolk supply. As long-term

20 photolabelling experiments are not possible in most of these species, we used

21 morphometric measurements of morphological regions on fixed samples as a proxy

22 for quantification of volumetric growth. Embryos for each species were fixed at

23 successive stages between the primitive streak/blastopore closure and the end of

24 somitogenesis, i.e throughout elongation of the posterior body. We built 3D surface

25 reconstructions and measured volume and length changes of the whole posterior

1　body, the unsegmented region (shaded red in Fig. 8A-D) and the two most anterior

2　body segments (shaded yellow in Fig. 8A-D) of the posterior body.

3

4　Both dogfish and mouse embryos showed an initial increase in unsegmented region

5　volume at early stages (Fig. 8B,D). On the contrary, in zebrafish and lamprey, this

6　region undergoes a continual reduction in volume throughout elongation (Fig. 8A,C).

7　The measurement of the volume of the two most anterior segments of the posterior

8　body in each species revealed that anterior volumetric growth is occurring in all

9　species, albeit at different intensities that correlate with the intensity of the overall

10　volumetric growth and elongation (Fig. 8H to compare with 8G and 8F). Taken

11　together, these results demonstrate that whilst posterior volumetric growth plays a

12　major role in the elongation of the posterior body of both mouse and dogfish

13　embryos, posterior body elongation in both lamprey and zebrafish embryos occurs

14　largely in the absence of posterior volumetric growth.

15

16　Measuring both length and volume changes of the whole posterior body reveals that

17　mice and dogfish, that have an internal development, undergo a larger overall

18　elongation and growth than lamprey and zebrafish who develop externally. This

19　suggests a positive triangular correlation between posterior volumetric growth,

20　overall elongation and volumetric growth and internal development.
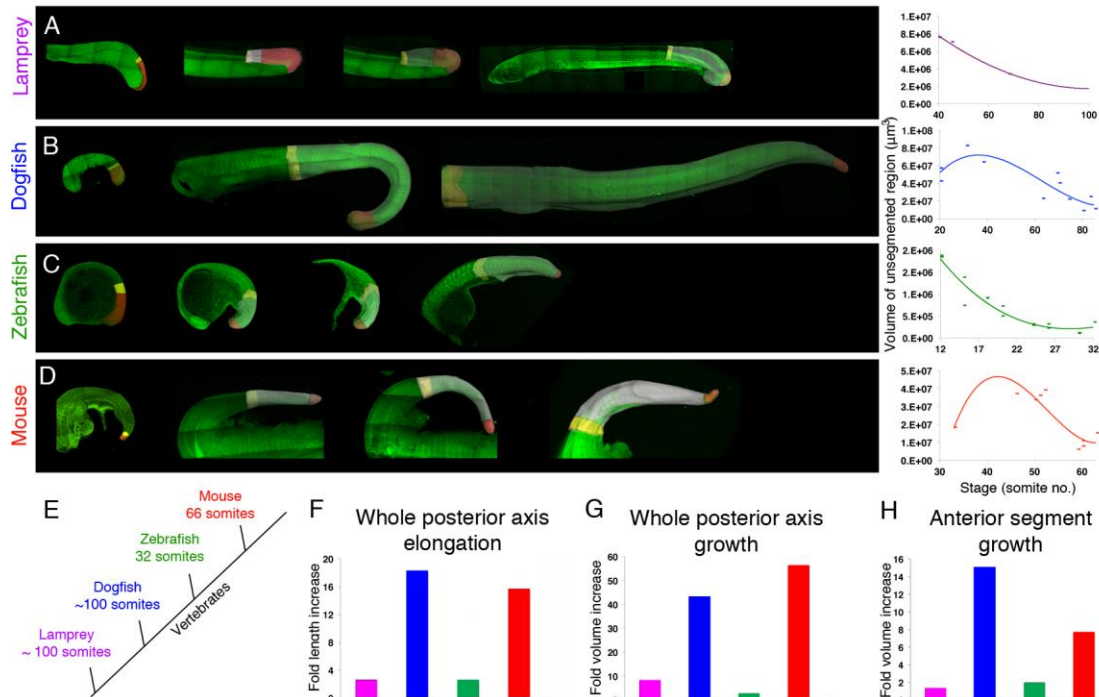
Figure 8. Comparative 3D morphometric analysis of posterior body elongation across vertebrates. (A-D) Maximal projections of tiled z-stacks of lamprey (A, n=7), dogfish (B, n=11), zebrafish (C, n=15) and mouse (D, n=10) embryos. All embryos were labelled with DAPI and phalloidin and are shown in lateral view with posterior to the right. Grey surface shows the segmented region, yellow the two most rostral segments of the posterior body and the red surface shows the unsegmented region. Plots of the unsegmented region volume over time (number of somites) are shown to the right for each species. (E) Simplified phylogeny for each species studied together with total somite number. (F-H) Fold change in length (F) and in volume (G) of the whole posterior body and fold change in volume of the two-most anterior segments (H) for each species. Purple bar= lamprey, blue= dogfish, green= zebrafish, red= mouse.

Discussion.

1 Our multi-scalar morphometric and cell tracking analyses show that posterior body

2 elongation in zebrafish is driven by i) an influx of cells initially lateral to the elongating

3 posterior body, ii) tissue deformation such as convergence-extension, mostly at the

4 tailbud-PSM transition and iii) volumetric growth in the segmented region, mostly in

5 the spinal cord and notochord. Our comparative analysis suggests that elongation

6 via posterior volumetric growth is linked to an internal mode of development with

7 increased energy supply.

8

9 **Zebrafish posterior body elongation is not driven by posterior volumetric**

10 **growth.**

11 If posterior growth were a major driver of elongation in zebrafish, one would expect

12 to observe volumetric growth of the unsegmented region. This is not what we

13 observe in our photolabelling experiments. However, we observe that tailbud cells

14 contribute to elongation mostly by rearrangement of pre-existing cells that undergo

15 convergence and extension as they enter the PSM. We do not rule out the existence

16 of slow-dividing self-renewing progenitors that provide cells to the elongating

17 posterior body. What our study shows is that these cells and their derivatives do not

18 generate sufficient additional tissue volume to drive elongation. Our fate mapping

19 shows that a large proportion of the cells that will make up the posterior body come

20 from regions lateral to the elongating posterior body that do or do not transit through

21 the tailbud.

22

23 The observation that the segmented region is a major contributor to posterior body

24 elongation explains the bi-phasic growth curve that is observed at the level of the

structure as a whole. During the no-growth phase, the spinal cord and notochord

volumetric growth, although occurring in anterior trunk structures (data not shown),

have not yet begun to occur within the posterior body. However, convergence and

extension of cells transiting from the tailbud to the PSM is well underway, resulting in

a thinning and lengthening of the posterior body in the absence of volumetric growth.

During the growth phase, in addition to continued thinning and lengthening, the dual

processes of spinal cord volumetric growth and notocord inflation have reached the

posterior body, resulting in an overall increase in posterior body volume and a

relative displacement of somitic and spinal cord cells.

Extensive volumetric growth and elongation during embryogenesis are associated with access to a large energy supply.

The limited overall and posterior volumetric growth in zebrafish and lamprey is in

contrast to both the mouse and dogfish where we observe large amounts of volume

increase in both unsegmented and segmented regions of the posterior body. The

dogfish embryo develops inside an egg case with a large yolk supply that is

reminiscent of avian embryos (Sauka-Spengler et al., 2003), and the mouse embryo

develops together with a large energy supply from the placenta. This is in contrast to

the larval-feeding zebrafish and lamprey embryos that have a limited access to

energy and must first establish a full axis in order to swim and find food to grow.

Therefore, overall volumetric growth appears to be associated with the increase in

energy that arises from an internal developmental mode. Posterior volumetric growth

in dogfish, an anamniote basal to the teleost fish with access to a large energy

supply, argues for a direct relationship between an increased maternal energy

1 supply and posterior volumetric growth, rather than for a late emergence of posterior

2 volumetric growth in amniotes. Whilst tissue deformations are likely to contribute in

3 all cases, an internal mode of development may have allowed for increased

4 contribution of volumetric growth behaviours in embryos such as mouse and dogfish.

5

6 **Conserved signaling pathways control different cell behaviors according to**

7 **elongation modes.**

8 Despite these differences, there is an apparent conserved requirement for both FGF

9 and Wnt signaling pathway components and downstream Cdx and Brachyury

10 transcription factors for posterior body elongation across a range of vertebrates

11 (Baker et al., 2010; Esterberg and Fritz, 2009; Marlow et al., 2004; Row and

12 Kimelman, 2009; Shimizu et al., 2005; Thorpe, 2005; Yang and Thorpe, 2011).

13 *Brachyury* is also expressed in the tailbud during elongation in dogfish and lamprey

14 embryos (Sauka-Spengler et al., 2003). Furthermore, *Brachyury, Wnt3*, *Wnt5* and

15 *Wnt6* are present within the tailbud of amphioxus embryos (Schubert et al., 2001),

16 considered to be the closest living relative of the chordate ancestor (Schubert et al.,

17 2006). A proliferative zone driving body elongation has been identified in several

18 invertebrate embryos where it has been shown to be associated with Wnt signaling

19 in spiders (McGregor et al., 2008), Artemia (Copf et al., 2004) and Tribolium

20 (Bolognesi et al., 2008; Copf et al., 2004; Schulz et al., 1998). In these different

21 model systems, these signaling pathways are required to direct cell fate decisions

22 and/or to regulate cellular flow as cells exit the tailbud and/or to maintain a posterior

23 growth/proliferative zone. Thus, it is likely that observed conserved molecular

24 mechanisms control different cellular behaviors according to different modes of

1   elongation. In the case of FGF signalling, this pathway has switched from a role in

2   posterior growth/proliferative zone maintenance in amniotes to a role in controlling

3   the cell movements in zebrafish.

4

5   **Methods**

6   **Fish strains and vertebrate embryos.**

7   Wild-type AB and zFUCCI green (Tg(EF1α:mAG-zGem(1/100))[rw0410h] (Sugiyama

8   et al., 2009) embryos were obtained from zebrafish (*Danio rerio*) lines maintained

9   following standard procedures (Westerfield, 2000). Embryos were raised at 28°C

10   and staged according to number of somites. mT/mG double-fluorescent Cre reporter

11   mice were utilized (Muzumdar et al., 2007). Dogfish (*S. canicula*) eggs and lamprey

12   (*L. fluviatilis*) embryos were produced by the Roscoff Marine Station. Embryos were

13   staged according to Ballard et al. (1993) and Tahara (1988), respectively.

14   **Preparation and fixation of zebrafish, mouse, dogfish and lamprey samples.**

15   Zebrafish wild-type embryos were injected at the one-cell stage with 500 pg of

16   H2B:mCherry and eGFP:CAAX box mRNAs (Hirsinger et al., 2015) and fixed in 4%

17   PFA for 20 minutes at RT. Dogfish embryos were collected from freshly killed *S.*

18   *canicula* females and kept in oxygenated sea water at 15°C until dissection and

19   fixation. Lamprey (*L. fluviatilis*) embryos were obtained by in vitro fertilization and

20   incubated at 18°C in oxygenated tap water. Dogfish, lamprey and mouse embryos

21   were fixed overnight in 4% PFA at 4°C and stored at −20°C in 100% methanol, until

22   re-hydratation and staining with 1µg/ml DAPI and 200nM phalloidin in PBS-0.01%

23   Tween overnight at 4 ^{0}C.

1

Imaging of fixed samples

Fixed zebrafish embryos were embedded in 1% low melting point agarose and

imaged either on a Zeiss Lightsheet Z.1 microscope or on a Leica SP5 confocal.

Lamprey embryos were embedded in 1% low melting point agarose and imaged

using a Leica SP5 confocal. Mouse and dogfish embryos were mounted in small

chambers containing RapidClear solution (Sunjin labs) and imaged on a Zeiss LSM

7 MP multiphoton microscope. Images were tiled and automatically stitched together

using the manufacturer software.

Zebrafish embryo injections and drug treatment.

500 pg of the following mRNAs were injected in one-cell stage embryos: cytoplasmic

KikGR (Hatta et al., 2006), nuclear-targeted nls-KikGR (kind gift of Ian Scott),

nuclear-targeted H2B:mCherry with/without membrane-localized eGFP:CAAX box

(Hirsinger et al., 2015). mRNA-injected embryos were incubated in either 500 µM

DMSO, 200 µM, 500 µM SU5402 (SIGMA SML0443-5MG) or 20 µM PD173074

(SIGMA P2499) from the 10- to the 32-somite stage. 90% epiboly or 12-somite stage

Live imaging and mapping of the prospective posterior body

Embryos were embedded in a small drop of 1% low melting point agarose within the

central glass ring of a glass-bottomed petri dish (Mattek; 35mm petri dish, 10mm

microwell. No. 1.5 cover glass). The agarose surrounding the tailbud was then

removed using a pulled glass capillary and imaged on an inverted Leica SP5

confocal microscope with a 20X air objective. 10 to 20 nuclei were photo-converted

1 from green to red by exposing the cells to 10 200Hz scans of a 405 laser at 60X

2 zoom. Nuclei were tracked in 4D using the image analysis tool Imaris (Andor

3 technologies). Tracks were filtered to include tracks from 90% epiboly through to the

4 12-somite stage and manually corrected. Surface renderings were automatically

5 segmented on the green channel using the 'surface' tool in Imaris, and reference

6 points were added at 50μm intervals along the embryonic midline from the dorsal

7 blastopore. Two lines were measured to tracks at a boundary between either the

8 posterior body-fated cells and the non-axial epidermis, or between posterior body-

9 fated cells and anterior trunk-fated cells. 3- and 6-somite embryos imaged by light-

10 sheet microscopy were used to map the full complement of boundary points with the

11 use of midline reference points as described. Surface reconstructions were created

12 by manually drawing contours at 10μm intervals.

13

14 **Volume segmentation and morphometric analysis**

15 To segment posterior body volume we utilized the 'Manually create surface' function

16 of Imaris. Contours were manually drawn at 10μm intervals in z, bordering the last

17 formed anterior trunk somite boundary of each species (somite 12 for zebrafish, 33

18 for mouse, 40 for lamprey and 20 for dogfish (Richardson et al., 1998). For

19 unsegmented regions, we took everything posterior to the notochord. For the anterior

20 body segments, we used the somite boundary of the first two posterior body somites.

21 Measurement points were placed at every other somite boundary along the axis, and

22 the values summed to give the length of the posterior body at any given stage.

23 Height and width measurements were made at each length measurement point and

24 plotted as described in the main text.

1

2 For the photolabelling experiments, embryos were imaged as for the cell tracking

3 experiments. Surface renderings were automatically created based on the red

4 channel at consecutive stages through the movies. Volume, height and width

5 measurements were made as described above.

6

7 **Cell counts and calculation of index of dispersion**

8 All nuclei within each image stack were segmented using the Imaris 'spots' function.

9 Manually checking the segmentation revealed that a diameter of 4µm enabled the

10 optimum segmentation of all nuclei in the image. Individual nuclei of clones labelled

11 by photoconverting nls-KikGR were segmented as described above for cell counts.

12 For each nucleus, the distance to all other nuclei along x, y and z axes was

13 calculated and ordered. The mean distance of the six closest neighbours was

14 calculated for each nucleus within the cluster and the mean change calculated as the

15 index of dispersion for each labelled clone.

16

17 **Quantification of the proliferation levels in zFUCCI green embryos.**

18 zFUCCI green embryos were injected with nuclear mCherry mRNA at one-cell stage

19 and imaged as described above. At the formation of each additional somite between

20 the 12- and 20-somite stages, both the whole posterior body and tailbud (determined

21 as the undifferentiated region of the body posterior to the notochord) were

22 segmented in 3D as described above. For tissue specific counts, we first generated

23 tissue specific surface renderings from manually drawn contours at 10µm intervals

24 through the z-stack. These were then taken as 'cells' in the Imaris 'Cell' to count both

total nuclei (using the H2B:mCherry signal) and nuclei in S/M/G2 (using the zFUCCI

green signal) within each tissue region. Nuclei were automatically detected using the

Imaris 'spots' function and manually inspected for accuracy.

Hybridisation chain reaction for assessing Sprouty4 expression

Five antisense DNA probes were designed against the full length zebrafish *sprouty4*

mRNA sequence (Accession number NM_131826.1) as described in Choi et al.

(2014). Embryos incubated in either DMSO or with 200 µM SU5402 from the 10

somite to 32 somite stage were fixed overnight in 4% PFA at 4°C and then stained

according to Choi et al. (2014). Imaging was performed on a Zeiss 700 confocal with

identical imaging parameters: z-step 0.5683µm; 1024x1024 resolution; 63X oil

objective; 35% laser power at 488 nm; Gain 661; Digitial offset -2; Pixel dwell time

3.12µm.

1 Institut National de la Santé et de la Recherche Médicale (INSERM).

2 The authors declare no competing interests.

3

4 **Author Contribution**

5 BS, EH and JFN conceived the project. BS performed most of the experiments and

6 developed analytical assays. FD aided in performing morphometric measurements.

7 EH performed live imaging for gastrula stage fate maps. RL and SM aided in staging

8 and obtaining lamprey and dogfish embryos. BS and EH interpreted the results. BS

9 and EH wrote the paper.

10

1

Funding information

Supplementary data

13

14 **S1 Movie. Example movie to determine posterior and lateral limits of the prospective posterior**

15 **body.**

16

17 **S2 Movie. Example movie of cells tracked to determine their final position within the paraxial**

18 **mesoderm.**

19

20 **S3 Movie. Example 3D reconstructions of the posterior body.**

21

22 **S4 Movie. Example of photolabelling in the unsegmented region of the posterior body**

23

24 **S5 Movie. Example of photolabelling in spinal cord and pre-somitic mesoderm**

25

26 **S6 Movie. Example of photolabelling in tailbud as cells transition to the pre-somitic mesoderm**

27 **S7 Figure. Proportional volumes of the spinal cord, paraxial mesoderm and notochord with**

28 **respect to the whole posterior body. (**A-B) Confocal stacks of 15-somite stage embryos injected at

29 the one-cell stage with nuclear mCherry and membrane-bound eGFP mRNAs were used to build

30 surface reconstructions of the spinal cord (blue), paraxial mesoderm (green) and notochord (purple).

1   (C) Proportional volume of each tissue with respect to whole posterior body volume. Measurements

2   are from three embryos.

3

4   **References**

5   **Baker, K. D., Ramel, M. C. and Lekven, A. C.** (2010). A direct role for Wnt8 in
6   ventrolateral mesoderm patterning. *Dev. Dyn.* **239**, 2828–2836.

7   **Ballard, W. W., Mellinger, J. and Lechenault, H.** (1993). A series of normal stages
8   for development ofScyliorhinus canicula, the lesser spotted
9   dogfish(Chondrichthyes: Scyliorhinidae). *J. Exp. Zool.* **267**, 318–336.

10   **Beddington, R. S.** (1994). Induction of a second neural axis by the mouse node.
11   *Development* **120**, 613–620.

12   **Bénazéraf, B., François, P., Baker, R. E., Denans, N., Little, C. D. and Pourquié,**
13   **O.** (2010). A random cell motility gradient downstream of FGF controls
14   elongation of an amniote embryo. *Nature* **466**, 248–252.

15   **Boehm, B., Westerberg, H., Lesnicar-Pucko, G., Raja, S., Rautschka, M.,**
16   **Cotterell, J., Swoger, J. and Sharpe, J.** (2010). The Role of Spatially
17   Controlled Cell Proliferation in Limb Bud Morphogenesis. *PLoS Biol.* **8**,
18   e1000420.

19   **Bolognesi, R., Farzana, L., Fischer, T. D. and Brown, S. J.** (2008). Multiple Wnt
20   Genes Are Required for Segmentation in the Short-Germ Embryo of Tribolium
21   castaneum. *Curr. Biol.* **18**, 1624–1629.

22   **Bouldin, C. M., Snelson, C. D., Farr, G. H. and Kimelman, D.** (2014). Restricted
23   expression of cdc25a in the tailbud is essential for formation of the zebrafish
24   posterior body. *Genes Dev.* **28**, 384–395.

25   **Cambray, N. and Wilson, V.** (2002). Axial progenitors with extensive potency are
26   localised to the mouse chordoneural hinge. *Development* **129**, 4855–4866.

27   **Choi HMT, Chang JY, Trinh LA, Padilla JE, Fraser SE, Pierce NA.** (2010) Programmable
28   in situ amplification for multiplexed imaging of mRNA expression. *Nat Biotechnol.* **28**,
29   1208–1212.

30   **Choi HMT, Beck VA, Pierce NA.** (2014) Next-Generation in Situ Hybridization Chain
31   Reaction: Higher Gain, Lower Cost, Greater Durability. *ACS Nano. American*
32   *Chemical Society* **8**, 4284–4294.

Copf, T., Schröder, R. and Averof, M. (2004). Ancestral role of caudal genes in axis elongation and segmentation. *Proc. Natl. Acad. Sci. U. S. A.* **101**, 17711–17715.

Del Corral, R. D. and Storey, K. G. (2004). Opposing FGF and retinoid pathways: a signalling switch that controls differentiation and patterning onset in the extending vertebrate body axis. *BioEssays* **26**, 857–869.

Ellis, K., Hoffman, B. D. and Bagnat, M. (2013). The vacuole within: how cellular organization dictates notochord function. *Bioarchitecture* **3**, 64–68.

Esterberg, R. and Fritz, A. (2009). dlx3b/4b are required for the formation of the preplacodal region and otic placode through local modulation of BMP activity. *Dev. Biol.* **325**, 189–199.

Glickman, N. S., Kimmel, C. B., Jones, M. A. and Adams, R. J. (2003). Shaping the zebrafish notochord. *Development* **130**, 873–887.

Gouti, M., Tsakiridis, A., Wymeersch, F. J., Huang, Y., Kleinjung, J., Wilson, V. and Briscoe, J. (2014). In Vitro Generation of Neuromesodermal Progenitors Reveals Distinct Roles for Wnt Signalling in the Specification of Spinal Cord and Paraxial Mesoderm Identity. *PLoS Biol.* **12**, e1001937.

Hatta, K., Tsujii, H. and Omura, T. (2006). Cell tracking using a photoconvertible fluorescent protein. *Nat. Protoc.* **1**, 960–967.

Hirsinger, E., Carvalho, JE., Chevalier, C., Lutfalla, G., Nicolas, JF., Peyriéras, N., Schubert, M. (2015) Expression of fluorescent proteins in Branchiostoma lanceolatum by mRNA injection into unfertilized oocytes. *J Vis Exp.* **95**, 52042.

Kanki, J. P. and Ho, R. K. (1997). The development of the posterior body in zebrafish. *Development* **124**, 881–893.

Lawton, A. K., Nandi, A., Stulberg, M. J., Dray, N., Sneddon, M. W., Pontius, W., Emonet, T. and Holley, S. A. (2013). Regulated tissue fluidity steers zebrafish body elongation. *Development* **140**, 573–582.

Marlow, F., Gonzalez, E. M., Yin, C., Rojo, C. and Solnica-Krezel, L. (2004). No tail co-operates with non-canonical Wnt signaling to regulate posterior body morphogenesis in zebrafish. *Development* **131**, 203–216.

Martin, B. L. and Kimelman, D. (2010). Brachyury establishes the embryonic mesodermal progenitor niche. *Genes Dev.* **24**, 2778–2783.

Martin, B. L. and Kimelman, D. (2012). Canonical Wnt Signaling Dynamically Controls Multiple Stem Cell Fate Decisions during Vertebrate Body Formation. *Dev. Cell* **22**, 223–232.

Mathis, L. and Nicolas, J. F. (2000). Different clonal dispersion in the rostral and caudal mouse central nervous system. *Development* **127**, 1277–1290.

McGregor, A. P., Pechmann, M., Schwager, E. E., Feitosa, N. M., Kruck, S., Aranda, M. and Damen, W. G. M. (2008). Wnt8 Is Required for Growth-Zone Establishment and Development of Opisthosomal Segments in a Spider. *Curr. Biol.* **18**, 1619–1623.

McGrew, M. J., Sherman, A., Lillico, S. G., Ellard, F. M., Radcliffe, P. A., Gilhooley, H. J., Mitrophanous, K. A., Cambray, N., Wilson, V. and Sang, H. (2008). Localised axial progenitor cell populations in the avian tail bud are not committed to a posterior Hox identity. *Development* **135**, 2289–2299.

Muzumdar, M. D., Tasic, B., Miyamichi, K., Li, L. and Luo, L. (2007). A global double-fluorescent Cre reporter mouse. *genesis* **45**, 593–605.

Neijts, R., Simmini, S., Giuliani, F., van Rooijen, C., & Deschamps, J. (2013). Region-specific regulation of posterior axial elongation during vertebrate embryogenesis. *Developmental Dynamics*, **243**, (1), 88–98.

Nicolas, J. F., Mathis, L., Bonnerot, C. and Saurin, W. (1996). Evidence in the mouse for self-renewing stem cells in the formation of a segmented longitudinal structure, the myotome. *Development* **122**, 2933–2946.

Olivera-Martinez, I., Harada, H., Halley, P. A. and Storey, K. G. (2012). Loss of FGF-Dependent Mesoderm Identity and Rise of Endogenous Retinoid Signalling Determine Cessation of Body Axis Elongation. *PLoS Biol.* **10**, e1001415.

Richardson, M. K., Allen, S. P., Wright, G. M., Raynaud, A. and Hanken, J. (1998). Somite number and vertebrate evolution. *Development* **125**, 151–160.

Riley, B. B., Sweet, E. M., Heck, R., Evans, A., Mcfarland, K. N., Warga, R. M. and Kane, D. A. (2010). Characterization of harpy/Rca1/emi1mutants: Patterning in the absence of cell division. *Dev. Dyn.* **239**, 828–843.

Row, R. H. and Kimelman, D. (2009). Bmp inhibition is necessary for post-gastrulation patterning and morphogenesis of the zebrafish tailbud. *Dev. Biol.* **329**, 55–63.

Sauka-Spengler, T., Baratte, B., Lepage, M. and Mazan, S. (2003). Characterization of Brachyury genes in the dogfish S. canicula and the lamprey L. fluviatilis. Insights into gastrulation in a chondrichthyan. *Dev. Biol.* **263**, 296–307.

Schubert, M., Holland, L. Z., Stokes, M. D. and Holland, N. D. (2001). Three Amphioxus Wnt Genes (AmphiWnt3, AmphiWnt5, and AmphiWnt6) Associated

with the Tail Bud: the Evolution of Somitogenesis in Chordates. *Dev. Biol.* **240**, 262–273.

Schubert, M., Escriva, H., Xavier-Neto, J. and Laudet, V. (2006). Amphioxus and tunicates as evolutionary model systems. *Trends Ecol. Evol.* **21**, 269–277.

Schulz, C., Schröder, R., Hausdorf, B., Wolff, C. and Tautz, D. (1998). A caudal homologue in the short germ band beetle Tribolium shows similarities to both, the Drosophila and the vertebrate caudal expression patterns. *Dev. Genes Evol.* **208**, 283–289.

Selleck, M. A. and Stern, C. D. (1991). Fate mapping and cell lineage analysis of Hensen's node in the chick embryo. *Development* **112**, 615–626.

Shimizu, T., Bae, Y. K., Muraoka, O. and Hibi, M. (2005). Interaction of Wnt and caudal-related genes in zebrafish posterior body formation. *Dev. Biol.* **279**, 125–141.

Sugiyama, M., Sakaue-Sawano, A., Iimura, T., Fukami, K., Kitaguchi, T., Kawakami, K., Okamoto, H., Higashijima, S. and Miyawaki, A. (2009). Illuminating cell-cycle progression in the developing zebrafish embryo. *Proc. Natl. Acad. Sci.* **106**, 20812–20817.

Tahara, Y. (1988). Normal Stages of Development in Lamprey, Lampetra reissneri (Dybowski). *Zoolog. Sci.* **5**, 109–118.

Thorpe, C. J. (2005). Wnt/ -catenin regulation of the Sp1-related transcription factor sp5l promotes tail development in zebrafish. *Development* **132**, 1763–1772.

Tsakiridis, A., Huang, Y., Blin, G., Skylaki, S., Wymeersch, F., Osorno, R., Economou, C., Karagianni, E., Zhao, S., Lowell, S., et al. (2014). Distinct Wnt-driven primitive streak-like populations reflect in vivo lineage precursors. *Development* **141**, 1209–1221.

Turner, D. a., Hayward, P. C., Baillie-Johnson, P., Rue, P., Broome, R., Faunes, F. and Martinez Arias, a. (2014). Wnt/ -catenin and FGF signalling direct the specification and maintenance of a neuromesodermal axial progenitor in ensembles of mouse embryonic stem cells. *Development* **141**, 4243–4253.

Tzouanacou, E., Wegener, A., Wymeersch, F. J., Wilson, V. and Nicolas, J.-F. (2009). Redefining the Progression of Lineage Segregations during Mammalian Embryogenesis by Clonal Analysis. *Dev. Cell* **17**, 365–376.

Westerfield M. (2000). The Zebrafish Book: A Guide for the Laboratory Use of Zebrafish (Danio rerio). Eugene, OR: University of Oregon Press.

1   **Yang, Y. and Thorpe, C.** (2011). BMP and non-canonical Wnt signaling are required
2   for inhibition of secondary tail formation in zebrafish. *Development* **138**, 2601–
3   2611.

4   **Zhang, L., Kendrick, C., Jülich, D. and Holley, S. A.** (2008). Cell cycle progression
5   is required for zebrafish somite morphogenesis but not segmentation clock
6   function. *Development* **135**, 2065–2070.

7